Cellulose-supported ferrihydrites for the removal of As(III), As(V) and Cr(VI) from mining-contaminated water

Anita Etale [a1], **Dineo Nhlane** [b], **Alseno Mosai** [b], **Yannick Nuapia** [b]

[a] Global Change Institute, University of the Witwatersrand, Johannesburg 2000, South Africa.

[b] Molecular Sciences Institute, School of Chemistry, University of the Witwatersrand, Johannesburg 2000, South Africa.

Abstract

Mining-induced water contamination remains a significant concern in many regions of the world due to the high concentrations of toxic ions often associated with it. In this study, cellulose-supported ferrihydrite composites (CNF-Fe) were prepared by seeding of ferrihydrite nanoparticles on cellulose nanofibres (CNFs) and employed for the removal of As(III), As(V) and Cr(VI) from contaminated water. The adsorbent was characterized by electron microscopy, gas adsorption, point of zero charge (pH_{PZC}), X-ray diffractometry (XRD), as well as infrared and Raman spectroscopy. Compared to parent CNFs, CNF-Fe adsorbents had lower crystallinity and a higher surface area: 218.76 m^2 g^{-1}. Further, with a pH_{PZC} of 6.3, CNF-Fe was positively charged at low pH and suitable for adsorption of anions at acidic conditions characteristic of acid mine drainage. In single-ions solutions, the removal efficiency of CNF-Fe was in the order Cr(VI)>As(V)>As(III) (i.e. 0.15, 0.12 and 0.11 mg g^{-1} respectively). Adsorption kinetics followed the pseudo second-order model and isotherms were best fitted by the Freundlich, Dubinin-Radushkevich, and Temkin models. However, when CNF-Fe was applied to AMD-contaminated water (pH 2.7), Cr(VI) uptake decreased to ~39% which was likely due to competition from sulphate and selenium ions. Nevertheless, the adsorbent displayed regeneration capabilities with ~98% As and ~45% Cr desorbed after 24 hours of treatment. Together, these results suggest that cellulose supported ferrihydrite composites can be applied in treatment of mine drainage-contaminated water in conjunction with pre-treatments that limit SO_4^{2-} and selenium concentrations.

Key words: acid mine drainage, arsenate, arsenite, chromate, hemp cellulose, cellulose nanofibres, TEMPO-oxidation

[1] Corresponding author: aetale@gmail.com, +27117176087.

Preprints (www.preprints.org) | NOT PEER-REVIEWED | Posted: 9 October 2020 doi:10.20944/preprints202010.0190.v1

1. Introduction

Acid mine drainage (AMD) presents a major challenge to regions of past mining activity through the contamination of ground and surface water (Naicker et al., 2003). AMD is often associated with mining of coal and metal sulphide ores, and the subsequent oxidative weathering of wastes generated through these processes. AMD has a significant impact on environmental quality and aquatic ecosystems due to its low pH conditions and the high concentrations of toxic metal and metalloid ions (Gray et al., 2000; Tutu, 2006). However, in regions with limited access to clean water, these impacts extend to human beings. A large proportion of the urban population in many cities of developing nations has no access to municipal services including water supply (Tutu and Stoler, 2016). Their dependence on surface and ground water makes mining and industrial water pollution a public health issue.

Arsenic and chromium present significant challenges in regions of previous mining activity. Here, oxidation of arsenopyrite in mine tailings results in the mobilisation of arsenic in surface waters, and concentrations as high as 34,000 mg L^{-1} have been reported in AMD-impacted surface waters (Nordstrom et al., 2000). Arsenic was recognised as a carcinogen as early at 1879 and is listed as one of the 10 chemicals of major public health concern by the World Health Organisation (WHO, 2019) exposure to arsenic is linked to such serious conditions as cardiovascular disease, diabetes, kidney failure, and developmental effects. Yet up to 140 million people in more than 50 countries are estimated to be exposed to excessive amounts of arsenic, mostly via contaminated water (Nordstrom, 2002). The WHO set a maximum limit for arsenic in drinking water at 10 µg L^{-1} close to two decades ago, even though this value is now recognised as too close to the lower confidence limit on the benchmark dose for 0.5 % response (World Health Organization, 2011).

Chromium enters the environment mainly from industrial activities such as metal plating and leather tanning. Nevertheless, mining and processing, in particular, of coal also contribute significantly to Cr(VI) pollution. Chromium concentrations in fly ash can be as high as 152 mg kg^{-1}. Its disposal in large quantities can result in elevated chromium concentrations in ground and surface water through leachate and run-off. Chromium is classified as a carcinogen, but exposure also results in erosive skin ulceration. The WHO limit for Cr(VI) in drinking water is set at 50 µg L^{-1} (World Health Organization, 2011).

In aquatic environments, Cr(VI) may exist as $HCrO_4^-$ and $Cr_2O_7^{2-}$ at pH 2-6, and CrO_4^{2-} at pH >6. The $H_2CrO_4^-$ form is less common as it occurs at pH < 0 (Saha et al., 2011). Arsenic, on the other hand, exists in a wide range of oxidation states, but arsenite (As_2O_3) and arsenate (AsO_4^{3-}) are the most common in water. As(V) dominates in aerobic environments, occurring in various protonation states including H_3AsO_4, $H_2AsO_4^-$, $HAsO_4^{2-}$, and AsO_4^{3-} (Smedley and Kinniburgh, 2002). Under reducing conditions, As(III) dominates as AsO_3^{3-}, and its protonated forms: H_3AsO_3 , $H_2AsO_3^-$, and $HAsO_3^{2-}$. A number of approaches to the removal of these ions from water have been demonstrated, including chemical oxidation/reduction (Morrison et al., 2002), membrane processes (Goetz et al., 2018), electrocoagulation (Hansen et al., 2006), and adsorption (Burton et al., 2009; Mamindy-Pajany et al., 2011; Rout et al., 2012; Sannino et al., 2009; Smith and Ghiassi, 2006). Adsorption offers multiple advantages including lower costs, choice of a wide range of materials as adsorbents, and the ability to increase adsorbent efficiency via functionalisation. Further, when nano-scale adsorbents are used, less material is required due to the greater surface areas and higher reactivities of materials at this scale.

Amorphous iron oxides, *e.g.* ferrihydrite, have long been applied for the adsorptive removal of various contaminants from water. Ferrihydrite is a porous, amorphous iron hydroxide, with particle sizes as low as 1.6 nm (Wang et al., 2013), and surface areas as high as 176-250 m^2 g^{-1}, (Müller et al., 2010; Rout et al., 2012)). The most widely reported nominal formula for ferrihydrite is $Fe_{10}O_{15}{\cdot}9H_2O$ (Schwertmann and Fechter, 1982), but other formulae including $Fe_4O_{12}(OH)_{12}{\cdot}12H_20)_{12}$, $Fe_{4.6}O_{12}(OH)_{12}{\cdot}12H_20)_{12}$, (Eggleton and Fitzpatrick, 1988) and $Fe_{8.2}O_{8.5}(OH)_{7.4}{\cdot}3H_2O$ (Michel et al., 2010) have also been proposed. Due to its large surface areas and affinity for various ions, ferrihydrite has been used for both large (Newcombe et al., 2008) and small-scale (Kleinert et al., 2011) water treatment in the removal of U(VI), As(III), As(V) Cd(II), Cu(II), Zn(II), Pb(II), Cr(VI), PO_4^{2-}, and SO_4^{2-} (Aredes et al., 2013; Johnston

Preprints (www.preprints.org) | NOT PEER-REVIEWED | Posted: 9 October 2020 doi:10.20944/preprints202010.0190.v1

and Chrysochoou, 2016, 2012; Leckie, J. O. Benjamin, M. M., Hayes, K., Kaufman, G., Altman, 1980; Müller et al., 2010; Rout et al., 2012; Waychunas et al., 1993; Zachara et al., 1987; Zhu et al., 2018).

Recently, cellulosic substrates including cellulose nanofibres (CNFs) and nanocrystals (CNCs) have attracted much attention due to their wide range of environmental engineering applications. With an annual production of over 7 million metric tonnes, cellulose is considered the most widely available natural polymer, and an inexhaustible source of raw material for environmental applications (Klemm et al., 2005). The environmental applications of cellulose, nanocrystals (CNCs) or nanofibres (CNFs) can be derived by oxidation with organic and inorganic acids alone or in concert with mechanical treatment (Espinosa et al., 2013; Foster et al., 2018). Production of CNFs usually involves mild oxidants *e.g.* sodium hypochlorite, and catalytic amounts of sodium bromide (NaBr), and TEMPO (2,2,6,6-tetramethylpiperidine-1-oxylradical) at pH 10-11, to produce fibres that are typically > 1 µm long and 20-100 nm wide (Hirota et al., 2010; Isogai et al., 2011; Saito et al., 2007; H. Sehaqui et al., 2016; Shinoda et al., 2012; Zhou et al., 2018) (Foster et al., 2018). CNFs are particularly attractive because the carboxylate moieties can be exploited for cation adsorption (Chai et al., 2020; Espinosa et al., 2013; Mautner et al., 2019; Silvério et al., 2013) or functionalised further e.g. using quaternary ammonium salts to target anionic contaminants (Acharya et al., 2014; Houssine Sehaqui et al., 2016; Shateri Khalil-Abad et al., 2009; Zaman et al., 2012).

Recent work has also shown that these negatively charged sites on CNFs can act as nanoparticle seeding sites. Zhu and colleagues (Zhu et al., 2017), reported copper nanoparticle deposits on TEMPO-oxidised CNFs exposed to Cu(II) solutions.

A major aim of the current study was, therefore, to exploit these properties of oxidised CNFs for the treatment of As and Cr contaminated water. CNFs prepared by TEMPO-mediated oxidation were used as supports for the seeding of ferrihydrite nanoparticles, and the composites employed for the removal of As(III), As(V) and Cr(VI). The ions were removed at pH 4 (As(V) and Cr(VI)) and pH 11 (As(III)). All three ions were in their most adsorbable forms at the selected pH values i.e. Cr(VI), As(V) and As(III) existed in solution primarily as $HCrO_4^-$, $H_2AsO_4^-$, and $AsO(OH)_2^-$, respectively.

2. Experimental

2.1 Materials

Sodium hydroxide (NaOH), sodium chlorite ($NaClO_2$), glacial acetic acid (CH_3COOH), sodium bromide (NaBr), sodium hypochlorite (NaClO, 12-15 % active chlorine) solution, 2,2,6,6-tetramethylpiperidine 1-oxyl radical (TEMPO), methanol, ferric chloride hexahydrate ($FeCl_3.6H_2O$), sodium sulphate (Na_2SO_4), disodium hydrogen arsenate (Na_2HAsO_4, purity > 90%), sodium arsenite ($NaAsO_2$, purity > 98%), and dipotassium chromate (K_2CrO_4) were analytical grade, and used without further purification. Solutions were prepared with double deionised water with a resistivity of 18.2 MΩ cm^{-1}. All glassware and polypropylene vials were washed, soaked in a 1M nitric acid bath for at least 24 hours, and rinsed with deionised water before use.

2.2 Extraction of cellulose fibres

Cellulose fibres were extracted from dried stems and branches of hemp plants soaked in water overnight before peeling off of fibres from the woody cores. Fibres were then subjected to alkali treatment (4 wt % NaOH) at 80 °C. After three treatment rounds, each lasting 2 hours, the cellulose fibres were bleached using equal parts of $NaClO_2$ (1.7 wt %) and acetate buffer (pH 4.8). The bleaching solution was prepared from 27 g NaOH and 75 mL glacial acetic acid, diluted to 1L. Three, 1-hour long, bleaching rounds were performed. The ratio of fibre to liquid was maintained at 1:20 for each bleaching round.

Preprints (www.preprints.org) | NOT PEER-REVIEWED | Posted: 9 October 2020 doi:10.20944/preprints202010.0190.v1

2.3 Synthesis of cellulose nanofibers by TEMPO-mediated oxidation

CNFs were synthesised by TEMPO-mediated oxidation according to the method described by (Montanari et al., 2005). TEMPO (30.86 mg) and NaBr (0.648 g) were added to cellulose fibres (2 g wet weight) suspended in 185 mL water. The suspension was mechanically agitated while NaClO (6 mL) was added dropwise to maintain the solution pH at 10.5 ± 0.5. After all the NaClO had been added, 0.5M NaOH was used to maintain the pH at the same level. The reaction was left to proceed for 24 hours at ambient temperature (21 ℃) and terminated by addition of methanol (15 mL). The pH of the suspension was adjusted to 7 using 0.5M HCl and water-soluble nanofibres retrieved by centrifuging the suspension and freeze-drying the residual.

2.4 Fabrication of cellulose-supported ferrihydrite adsorbents

The cellulose supported ferrihydrite adsorbent was fabricated by deposition of iron oxides onto CNFs (Mukherjee et al., 2019). Ferrihydrite was prepared by a modification of the method described by Davis and Leckie (1978). Briefly, freeze-dried CNFs (0.1 g) were dissolved in 10 mL of distilled water and sonicated for five minutes. The pH of the solution was then adjusted to 9 using 0.1 M NaOH, after which Na_2SO_4 (1 g) was added for ionic strength. Ferric chloride hexahydrate (5.406 g) dissolved in 20 mL distilled water was then added to this solution and the pH adjusted to 8 by dropwise addition of 0.2 M NaOH. The product was left to incubate overnight at room temperature (20 ℃) and recovered after three wash-centrifuge cycles. Each centrifuge cycle was 2 minutes long, at 2325 x *g*. The adsorbent was labelled CNF-Fe. For comparison, a plain ferrihydrite (without cellulose), and a CNF-Fe-1 (with half the mass of ferric ions i.e. 0.1 g cellulose, 0.5 g Na_2SO_4, and 2.703 g $FeCl_3.6H_2O$) were prepared.

2.4 Characterisation of CNF-Fe adsorbents

The morphology of cellulose-supported ferrihydrite absorbents was examined using transmission electron microscopy (FEI Tecnai G^2 Spirit TEM, Hillsboro, USA) operated at an acceleration voltage of 120 kV. Samples were prepared by sonicating ~1 mg of the adsorbent in 20 mL methanol for 30 minutes. An aliquot of the suspension was then dropped onto a carbon-coated grid and the methanol allowed to evaporate. Adsorbents were also imaged using a field emission scanning electron microscope (Zeiss Sigma 300 FESEM; Jena, Germany) after application of a gold/palladium coating.

Raman spectra were acquired using the 514.5 nm line of a Lexel Model 95-SHG argon ion laser of a Horiba LabRAM HR Raman spectrometer (Tokyo, Japan) equipped with an Olympus BX41 microscope attachment. The incident light was focused onto the sample using a long working distance 100x objective, and the backscattered light was dispersed via a 600 lines mm^{-1} grating onto a liquid nitrogen cooled CCD detector. The sample was exposed to 80,000 W/ cm^2 for an accumulation time of 180 seconds. Duplicate spectra were collected in order to obtain spectra with optimal signal to noise ratio. Readings were recorded using LabSpec V5 software from 100-1900 cm^{-1} with a step-size of 1.9 cm^{-1}.

Fourier transform infrared spectra were recorded in the range 4000–500 cm^{-1} using a Tensor 27 Infrared Spectrometer (Massachusetts, USA). X-ray diffraction analysis was performed on a Bruker D2 diffractometer (Cu-Kα) (Johannesburg, South Africa) at a scanning range of 10° - 90° (2θ), a step size of 0.026 and step time of 37 seconds. The surface area of the adsorbents was determined using nitrogen adsorption isotherms measured with a Micrometrics ASAP 2010 adsorption analyser (Georgia, USA) at liquid nitrogen temperature. Samples were degassed at 100℃ for 10 hours prior to measurements. The Brunauer−Emmett−Teller (BET) surface area was estimated from the relative pressure range between 0.01 and 0.99 and pore size distribution curves were calculated by the Barrett−Joyner−Halenda method from the adsorption branch.

The pH_{pzc} of the CNFs and cellulose-supported ferrihydrite adsorbents were determined by salt titration method (Udoetok et al., 2016). For this, a 0.01M NaCl solution was prepared and 25 mL aliquots transferred to five polypropylene tubes. The pH of these solutions was then adjusted between 2 and 10 using 0.1M NaOH and 0.1M HNO_3 so that each tube had a different pH value. CNF and CNF-Fe and CNF-Fe-1 (0.1 g) were then added to the

Preprints (www.preprints.org) | NOT PEER-REVIEWED | Posted: 9 October 2020 doi:10.20944/preprints202010.0190.v1

NaCl solutions and suspensions equilibrated on a horizontal shaker for 48 hours. The final pH of each solution was plotted against the initial pH of the solutions and the pH_{pzc} for each material determined from intersection points.

The carboxyl concentrations of the CNFs, CNF-Fe and CNF-Fe-1 were determined by conductometric titration (Ji et al., 2019). About 0.1 g of CNF / CNF-Fe was dissolved in 55 mL distilled water and the pH of solutions adjusted to 2.5- 3 using 0.1M HCl. After stirring for 10 minutes, the suspensions were titrated using freshly prepared 0.01M NaOH at a rate of 0.1 mL minute $^{-1}$. The carboxyl content of CNFs and CNF-Fe were calculated using Equation 1 below:

$$C_{COOH} = \frac{C_{NaOH}V_1 - C_{NaOH}V_2}{M} \quad (1)$$

Where V_1 and V_2 were the volume of the consumed NaOH when the conductivity became stable and started to increase, respectively; M was the oven-dry weight of the materials.

2.5. Adsorption experiments

Preliminary adsorption experiments showed that CNF-Fe was more efficient at removal of As(III), As(V) and Cr(VI) under the selected reaction conditions, compared to CNF-Fe-1 (Supplementary information). It was, therefore, selected for subsequent batch adsorption studies which were performed separately for As(III), As(V) and Cr(VI). Solutions of As(III) (7.42 mg L^{-1}), As(V) (2.78 mg L^{-1}) and Cr(VI) (7.75 mg L^{-1}) solutions were prepared from $NaAsO_2$, Na_2HAsO_4, and K_2CrO_4, respectively. Removal efficiencies of CNF-Fe for As(III), As(V) and Cr(VI) were determined by exposing it (30 mg) to 25 mL solutions of deionised water spiked with these ions, in polypropylene centrifuge tubes.

Removal was investigated at pH 4 for As(V) and Cr(VI), and at pH 11 for As(III), with pH adjustments made using 0.1M HNO_3 and 0.1M NaOH. Reaction kinetics were determined by quantifying ion removal after reaction durations that ranged from five minutes to 24 hours, and isotherms by exposing a constant mass of the adsorbent (30 mg) to varying concentrations of As and Cr. At the end of reactions, solutions were filtered using 0.22 µm polyvinylidene difluoride (PVDF) syringe filters, and the filtrate assayed for total As and Cr by inductively-coupled plasma-optical emission spectroscopy (ICP-OES, Spectro Instruments, Kleve, Germany).

The equilibrium removal efficiency (q_e; mg g^{-1}) of CNF-Fe composites for As(III), A(V) and Cr(VI) was calculated using Equation 2:

$$q_e = \frac{C_o - C_e}{m} \times V \quad (2)$$

Where, C_0 and Ce are the initial and final concentration of the ions in solution (mg L^{-1}), respectively, V is the volume of the solution (L) and m is the mass of the adsorbent (g).

2.6 Application to real mine water

Adsorption efficiency was also tested on field samples of mine-drainage contaminated water in batch and gravity column studies. For Batch studies, 0.1 g of CNF-Fe adsorbent was contacted with AMD-contaminated water (pH 2.7), on a horizontal rotary shaker, for 4 hours (Previous experiments had shown this duration to be sufficient for equilibrium). After this time, the samples were centrifuged, filtered, acidified and stored at 4 °C before analysis of As and Cr concentrations. For column studies, a 30 mm diameter glass column was packed with 1 g plain cellulose (to minimise adsorbent loss) and 0.1g CNF-Fe. AMD-contaminated water was then poured into the column and the rate of filtrate production recorded. The filtrate was then analysed for As and Cr removal by ICP-OES.

Preprints (www.preprints.org) | NOT PEER-REVIEWED | Posted: 9 October 2020 doi:10.20944/preprints202010.0190.v1

2.7 Desorption of Cr and As from CNF-Fe sorbent

The desorption of As and Cr from the CNF-Fe sorbent was assessed using the standardized procedures for metal leaching (method 1311) (USEPA, 1992). After adsorption experiments, 1.98 g of adsorbents were suspended in 25 mL of extraction fluid (5.7 mL glacial acid in 1 L of water), at pH 2.88, and shaken for 24 hours on a horizontal shaker. Slurries were then centrifuged at 3000 rpm for 20 minutes. Precipitates were dried in ambient conditions while the supernatant was filtered through 0.22 µm PVDF filters, acidified using 5% HNO_3, and analysed by ICP-OES.

3. Results and discussion

i. Material characterisation

Electron micrographs confirmed the structures of hemp CNFs and CNF-Fe composite. Scanning electron micrographs of hemp CNFs (Figure 1a) revealed agglomerations of plate-like particles, but which were no longer visible in the CNF-Fe composites (Figure 1b). Transmission electron micrographs of CNF-Fe composites (Figure 1c) showed that they comprised agglomerations of nano-sized particles. The BET surface areas of CNFs, CNF-Fe and iron oxyhydroxide were 2.23, 5.12, and 218.67 $m^2\ g^{-1}$, respectively. An examination of the hysteresis plots (see Supplementary information) of all three materials gave further insights into their structural composition. N_2 adsorption-desorption by hemp CNFs was characterised type 3 hysteresis typical of loose aggregates of plate-like particles (Thommes et al., 2015). Gas adsorption by iron oxyhydroxide particles, on the other hand was characterised by Type 4a hysteresis, indicating that these particles had narrow, slit-shaped micropores. The CNF-Fe composite had a Type 2 hysteresis, implying that the material had narrow interconnected pores , which could be the result of iron oxide deposition within the inter-platelet spaces of the CNFs.

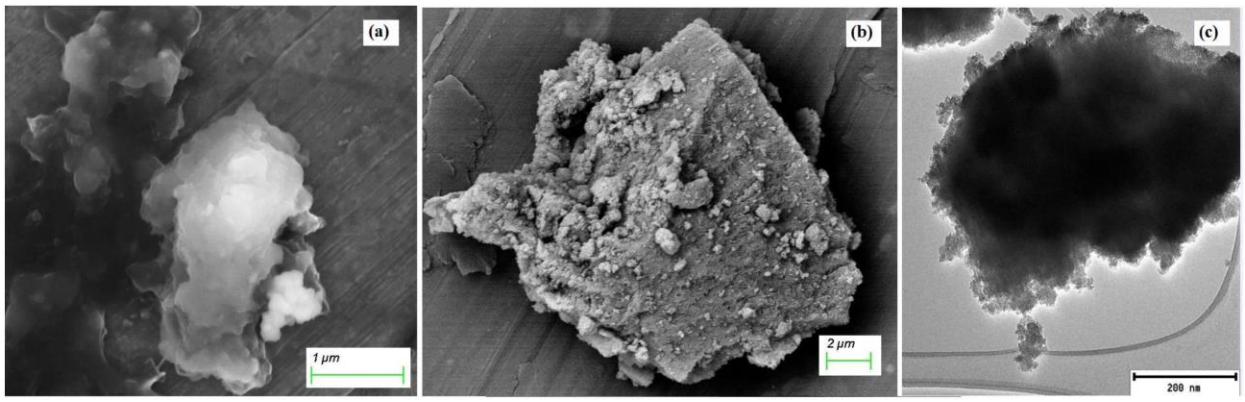

Figure 1: (a) Scanning electron micrograph of hemp CNFs. (b) and (c) are the scanning and electron micrographs, respectively, of CNF-Fe.

The infrared spectra of CNFs derived from TEMPO oxidation of hemp cellulose as well as those of CNF-Fe and iron oxyhydroxide are shown in Figure 2. Spectra of CNFs (Figure 2-i) showed absorption bands at 1625 and 970 cm^{-1} attributed to sodium carboxylate groups formed from TEMPO-mediated oxidation of C6 hydroxyls (Coates, 2004). Ferrihydrite spectra were characterised by broad maxima at 3200 cm^{-1} due in part to adsorbed water, which also gave rise to the band at 1643 cm^{-1} (Russel, 1979). A weak, broad deformation band at 852 cm^{-1}, and a broad inflection at ~ 1000 cm^{-1} from vibration of surface -OH moieties on the iron oxyhydroxide were also observed (Figure 2 -ii). Extensive similarities in the spectra of the ferrihydrite and the CNF-Fe composite, particularly in the 3500-1200 region confirmed the presence of ferrihydrite in the complex. Notably, bonding between ferrihydrite and CNFs is confirmed by the absence of ferrihydrite OH group vibrations at 852 cm^{-1} in the CNF-Fe composite, suggesting the formation of

Preprints (www.preprints.org) | NOT PEER-REVIEWED | Posted: 9 October 2020 doi:10.20944/preprints202010.0190.v1

CNF-O-FeOOH bonds between the CNFs and ferrihydrite. Finally, although sulphate ions (residual from synthesis) are present in CNF-Fe composite, their clear delineation is hampered by overlap with OH vibrations. Nevertheless, identification of residual sulphate (at 980 cm^{-1}) was possible using Raman spectroscopy (Figure 3).

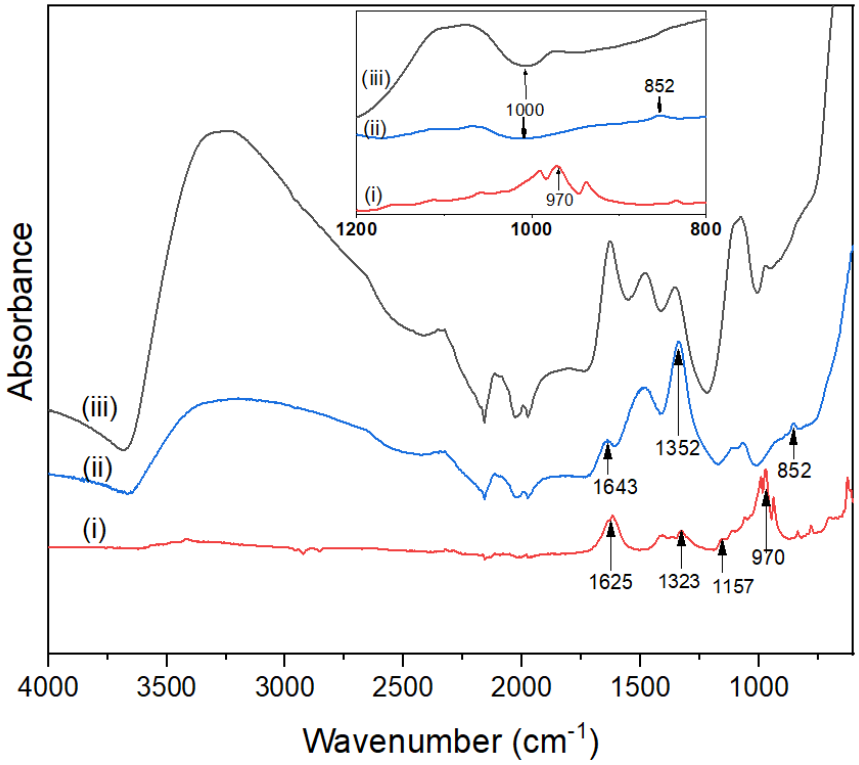

Figure 2: FTIR spectra of (i) hemp CNFs, (ii) iron oxyhydroxide and (iii) CNF-Fe composite adsorbent from iron oxyhydroxide and hemp CNFs. Inset: adsorption in the 1200-800 cm^{-1} region highlighting the regions of hydroxyl and carboxylate absorption.

Raman spectroscopy was also used to determine the specific ferrihydrite phase in CNF-Fe. The spectra (Figure 3) comprised bands characteristic of 2-line ferrihydrite i.e. broad, weak bands at ~ 360, and ~510, and a stronger band at ~712 cm^{-1} (Mazzetti and Thistlethwaite, 2002; Müller et al., 2010). As such, the iron oxyhydroxide phase deposited onto the cellulose framework was 2-line ferrihydrite. Additional confirmation of the starting material being ferrihydrite was provided by the appearance of bands characteristic of hematite i.e.~227, ~293 and ~399 cm^{-1} (Mazzetti and Thistlethwaite, 2002), when the material was exposed to a higher laser power (100,000 w/cm^2) (Figure 3-ii). Finally, the broad band at ~1380 cm^{-1} is due to stretching and bending vibrations of cellulose C-O-H bonds (Foster et al., 2018), and that at ~980 cm^{-1} is due to residual sulphate from synthesis (Müller et al., 2010).

Preprints (www.preprints.org) | NOT PEER-REVIEWED | Posted: 9 October 2020 doi:10.20944/preprints202010.0190.v1

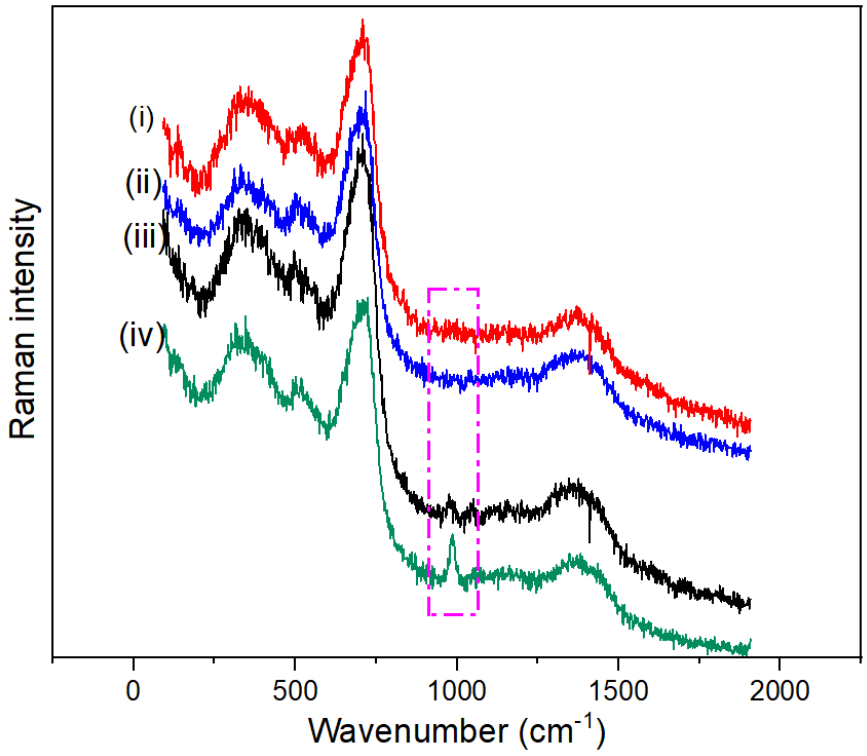

Figure 3: Raman spectra of (i) the CNF-Fe adsorbent confirming the iron oxyhydroxide as 2-line ferrihydrite and (ii-iv) spectra showing transformation of the ferrihydrite to hematite after exposure to 100,000 W/cm^2 laser power.

X-ray diffractograms showed that hemp cellulose fibres were largely amorphous, with the characteristic cellulose peaks at 16 and 23 2θ. In contrast, the CNFs derived from TEMPO-mediated oxidation of the cellulose displayed more crystallinity (Figure 4b) but this was again lost in the CNF-Fe composite. The diffractogram of the CNF-Fe composite (Figure 4c) was characterised by broad maxima centred at 18.6 2θ which may be due to an amalgamation of the CNF peak at 16 2θ, and the ferrihydrite peak at 16.55 2θ which corresponds to the (110) plane of Cellulose I (Rout et al., 2012).

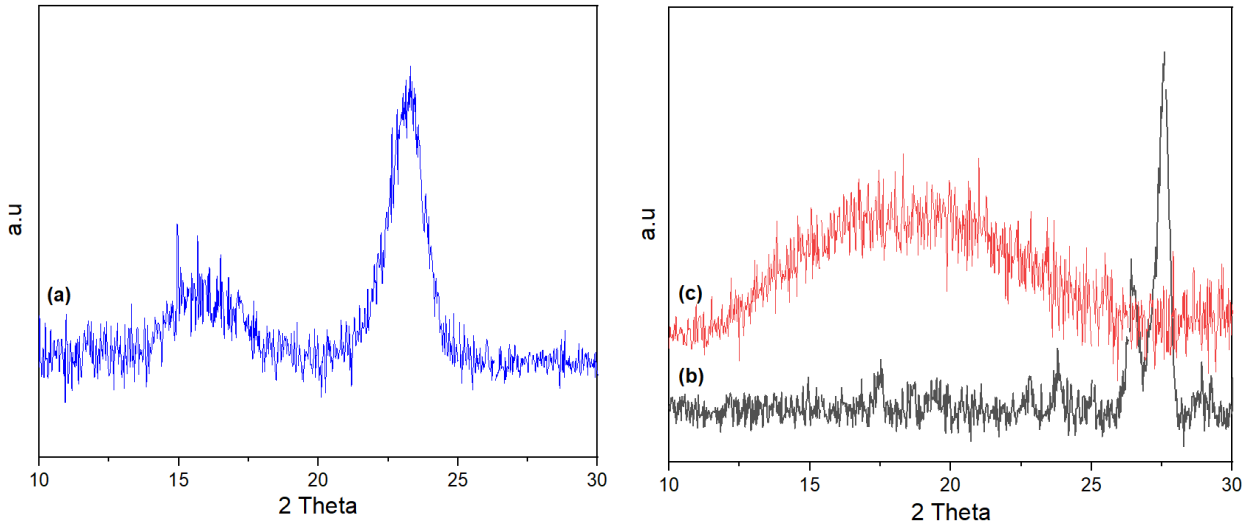

Figure 4: X-ray diffractograms of (a) hemp cellulose (b) CNFs from TEMPO-mediated oxidation of hemp cellulose (c) CNF-Fe composite

Preprints (www.preprints.org) | NOT PEER-REVIEWED | Posted: 9 October 2020 doi:10.20944/preprints202010.0190.v1

The pH_{pzc} of CNF-Fe was determined as 6.3, which was slightly lower than that of a synthetic 2-line ferrihydrite reported by Wang and colleagues: 8.7 (Wang et al., 2013). We surmise that this may be due to the presence of sulphate ions in the ferrihydrite synthesised in this study as evidenced by Raman spectroscopy; Schwertmann and Fechter (1982) found that the presence of anions lowered the pH_{pzc} of ferrihydrites.

With respect to carboxylate content, the data were in line with expected values. Carboxyl concentration decreased with increasing deposition of ferrihydrite. Plain CNF had a COO^- concentration of 0.985 mmol g^{-1} while CNF-Fe with 0.5 M ferric chloride had a COO^- concentration of 0.699 mmol g^{-1}, and CNF-Fe with 1 M ferric chloride had a COO^- concentration of 0.599 mmol g^{-1}. This suggests that ferric ions were bound to the COO^- groups of CNFs and explains the decrease observed when ferric ions were added to CNF solution.

ii. Adsorption by CNF-Fe composite

The uptake of As(V), Cr(VI) was examined at pH 4 while that of As(III) was examined at pH 11 using 0.03 g CNF-Fe composites. Anion solution concentrations varied thus: 2.52 - 14.49 mg L^{-1} for As (III), 0.99 – 14.10 mg L^{-1} for As(V), and 10.6 – 80.0 mg L^{-1} for Cr(VI). The contact time was kept constant at 240 minutes for all reactions. As shown in Figure 5, equilibrium adsorption capacities (q_e) of the CNF-Fe adsorbent increased with increasing initial concentrations, which is likely due to the increased drive for diffusion towards adsorbent surfaces at higher ion concentrations (Ho and Mckay, 2004). The results also indicated that equilibrium uptake was in the order Cr(VI) > As(V) > As(III).

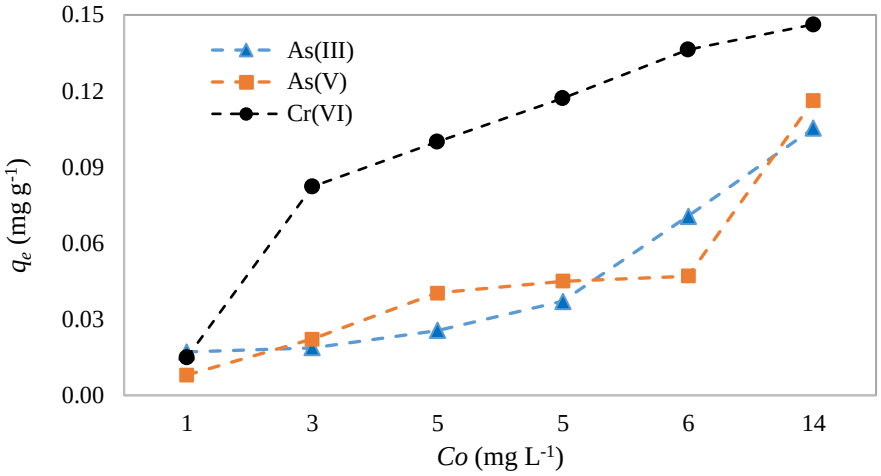

Figure 5: The effect of adsorbate dose on removal of As(III), As(V) and Cr(VI) removal by CNF-Fe adsorbent. Conditions: adsorbent mass: 0.03g; As(V) and Cr (VI): pH 4; As(III): pH 11; contact time = 240 minutes.

Adsorption isotherms

The mechanisms by which As(III), As(V) and Cr(VI) were adsorbed by cellulose-supported ferrihydrites were investigated by fitting adsorption isotherm data to Langmuir, Freundlich, Dubinin-Radushkevich (D-R) and Temkin isotherm models. The Langmuir isotherm describes data where the adsorbate molecules interact with active sites that have similar energies, leading to monolayer surface coverage, with no interactions between adsorbate molecules and neighbouring sites (Leckie, J. O. Benjamin, M. M., Hayes, K., Kaufman, G., Altman, 1980).The Langmuir isotherm model can be expressed as Equation 3:

Preprints (www.preprints.org) | NOT PEER-REVIEWED | Posted: 9 October 2020 doi:10.20944/preprints202010.0190.v1

$$\frac{C_e}{q_e} = \left(\frac{1}{q_m}\right) C_e + \left(\frac{1}{K_L q_m}\right) \quad (3)$$

where q_e (mg g^{-1}) is the quantity of the adsorbate adsorbed per gram of adsorbent at equilibrium, q_m (mg g^{-1}) is the maximum monolayer coverage capacity and K_L (L mol^{-1}) is the Langmuir constant.

The Freundlich isotherm model is based on the multilayer adsorption of adsorbate molecules onto a heterogeneous surface and can be expressed as Equation 4 where K_f ((mg g^{-1})/(mol L^{-1})$^{1/n}$) is the Freundlich isotherm constant, and n is the adsorption intensity (Leckie, J. O. Benjamin, M. M., Hayes, K., Kaufman, G., Altman, 1980):

$$q_e = K_F C_e^{\frac{1}{n}} \quad (4)$$

The D-R isotherm (Equation 5) is an empirical model which can express adsorption onto homogeneous and heterogeneous surfaces (Dubinin, 1947), predicting whether the adsorption processes is physical or chemical based on values of the mean free energy of adsorption (Hutson and Yang, 1997).

$$ln q_e = ln X_m - K_{DR} \varepsilon^2 \quad (5)$$

Where $\varepsilon = RT ln\left(1 + \frac{1}{C_e}\right)$ (6)

$K_{D\text{-}R}$ (mol^2 (kJ^2)$^{-1}$) is the Dubinin-Radushkevich isotherm constant, X_m (mg g^{-1}) is theoretical isotherm saturation capacity, ε is the Polanyi constant, R is the universal gas constant (8.314 J (mol K)$^{-1}$) and T (K) is temperature. The mean free energy change, E_s (kJ mol^{-1}), which is the energy required to transfer one mole of ion from infinity in the solution to the solid surface can be calculated using Equation 7.

$$E_s = \frac{1}{\sqrt{2K_{D-R}}} \quad (7)$$

The Temkin isotherm model takes the adsorbent-adsorbate interactions into account and assumes that the free energy of adsorption is a function of the surface coverage was also used (Raven et al., 1998). It is expressed as in Equation 11 where K_T (L mg^{-1}) is the equilibrium binding constant, b is the Temkin isotherm constant.

$$q_e = B\ lnK_T + B\ lnC_e \quad (8)$$

B (J mol^{-1}) is related to the heat of adsorption, and is calculated: $B = \frac{RT}{b_T}$ (9)

The results (Table 1) showed that As(III) and As(V) were better described by the Freundlich isotherm model, indicating that their uptake by CNF-Fe occurred onto energetically heterogeneous sorption sites. Furthermore, the value of n showed that the adsorption was favourable. The mean free energy change (*Es*), for all three ions was between 8 and 16 kJ mol^{-1}, suggesting that the interaction between the ions and the adsorbent was due to chemisorption / ion exchange process.

Uptake of Cr(VI) was also to a heterogeneous surface, going by the fit of data to the Freundlich isotherm. However, the adsorption was best explained by the Temkin isotherm which suggests that the adsorption of Cr(VI) to CNF-Fe was accompanied by a linear reduction in the heat of adsorption (Aharoni and Ungarish, 1977).

Preprints (www.preprints.org) | NOT PEER-REVIEWED | Posted: 9 October 2020 doi:10.20944/preprints202010.0190.v1

Table 1: Isotherm parameters for the adsorption of As(III), As(V) and Cr(VI) by cellulose-supported ferrihydrites

Isotherm	Parameter	As(III)	As(V)	Cr(VI)
Langmuir	q_m (mg g^{-1})	4.56 x 10^{-6}	1.21 x 10^{-5}	1.45 x 10^{-5}
	K_L (L mol^{-1})	2.81 x 10^{5}	6.08 x 10^{4}	4.40 x 10^{3}
	R^2	0.002	0.90	0.30
Freundlich	K_F ((mg g^{-1}) (mg $L^{-1})^{1/n}$)	1.02	0.99	1.06
	n	3.43	4.11	3.59
	R^2	0.81	0.97	0.91
Dubinin–Radushkevich	K_{D-R}, (mol^2 J^{-2})	0.004	0.003	0.006
	$q_{m\ (cal)}$ (mmol g^{-1})	1.02	0.69	1.09
	E_s, kJ mol^{-1}	10.74	13.17	9.06
	R^2	0.80	0.97	0.92
Temkin	K_T	2.1 x 10^{5}	1.1 x 10^{7}	8.3 x 10^{3}
	b_T	5.2 x 10^{4}	1.3 x 10^{5}	1.8 x 10^{4}
	R^2	0.67	0.86	0.99

Adsorption kinetics

The effect of time on metal uptake by cellulose-supported ferrihydrites was examined using pseudo-first order, pseudo-second order and Elovich kinetic models expressed as Equations 10, 11 and 12 respectively.

$$\log(q_e - q_t) = log q_e - \frac{k_1 t}{2.303} \quad (10)$$

$$\frac{t}{q_t} = \frac{1}{k_2 {q_e}^2} + \frac{1}{q_e}\mathrm{t} \quad (11)$$

$$q_t = \frac{1}{\beta}\ln(\alpha\beta) + \frac{1}{\beta}\ln(t) \quad (12)$$

where q_t (mg g^{-1}) is the amount of metal adsorbed at time t, k_1 (min^{-1}) is the pseudo first-order rate constant. For the pseudo second-order equation, k_2 (g mg^{-1} min^{-1}) is rate constant, α (mg $g^{-1}min^{-1}$) represents the chemisorption rate and available adsorption surface, and β (mg g^{-1}) is related to surface coverage. Correlation coefficients (R^2), and experimental and calculated q_e values, were used to determine model fit(Ho and Mckay, 2004).

The results indicated that, based on R^2 values and the calculated and experimental q_e values (Table 2), uptake of all three ions by CNF-Fe was best described by the pseudo-second order kinetic model. Adsorption was therefore via chemisorption.

Preprints (www.preprints.org) | NOT PEER-REVIEWED | Posted: 9 October 2020 doi:10.20944/preprints202010.0190.v1

Table 2: Kinetic parameters for the adsorption of As(III), As(V) and Cr(VI) by cellulose-supported ferrihydrite

Model	Parameter	As(III)	As(V)	Cr(VI)
Pseudo-first order	k_1 (min $^{-1}$)	11.4	7.50	7.04
	$q_{e,\ cal}$ (mg g^{-1})	0.086	0.01	0.16
	$q_{e,\ exp}$ (mg g^{-1})	0.82	0.30	0.79
	R^2	0.42	0.16	0.95
Pseudo-second order	k_2 (g mg^{-1} min $^{-1}$)	1.58	0.99	0.95
	$q_{e,\ cal}$ (mg g^{-1})	0.82	0.29	0.74
	$q_{e,\ exp}$ (mg g^{-1})	0.82	0.30	0.79
	R^2	0.99	0.99	0.99
Elovich	α (g mg^{-1} min^{-1})	8.7 x 10^{-5}	2.3 x 10^{-5}	62.2
	β 1/b (g mg^{-1})	37.7	1127	28.3
	R^2	0.78	0.80	0.83

iii. Post-sorption spectroscopic characterisation of adsorbents

Adsorbents were characterised after exposure to test ions in order to elucidate modes of arsenic and chromium uptake by CNF-Fe. The major change noted in the spectra of post-adsorption materials was centred on the inflection around 1000 cm^{-1}, attributed to surface OH groups. The spectra showed a reduction in IR absorption in this region for both As (III) and As(V), although the reduction was higher is the former (Figure 6a). Uptake of both ions by ferrihydrite occurs via ligand exchange and is therefore accompanied by the release of OH ions from the ferrihydrite surface (Jain et al., 1999).

Two factors explain the differences in post-adsorption spectra for As(III) and As(V). The first involves abundance of binding sites: Fe-OH and Fe-OH$_2$ sites are available for uptake of As(V) at pH 4, but only Fe-OH sites were available at pH 11 for uptake of As(III). Second, the concentration of As(III) ions was far higher than that of As(V) i.e. 99 µM As(III) and 37 µM As(V) (Speciation diagrams are provided in the Supplementary Information). Together, this implies that for As(V), there were more adsorption sites for less ions, whereas the opposite was the case for As(III. As such, even after As(V) uptake, a high number of OH ions were still available at the sorbent surface, hence the relatively small difference in pre- and post As(V) uptake spectra. In contrast, a small number of sorption sites for higher arsenite concentrations resulted in the exchange of a significant portion of OH ions from the CNF-Fe surface, hence the notable change in the CNF-Fe spectra after uptake of As(III) ions.

Preprints (www.preprints.org) | NOT PEER-REVIEWED | Posted: 9 October 2020 doi:10.20944/preprints202010.0190.v1

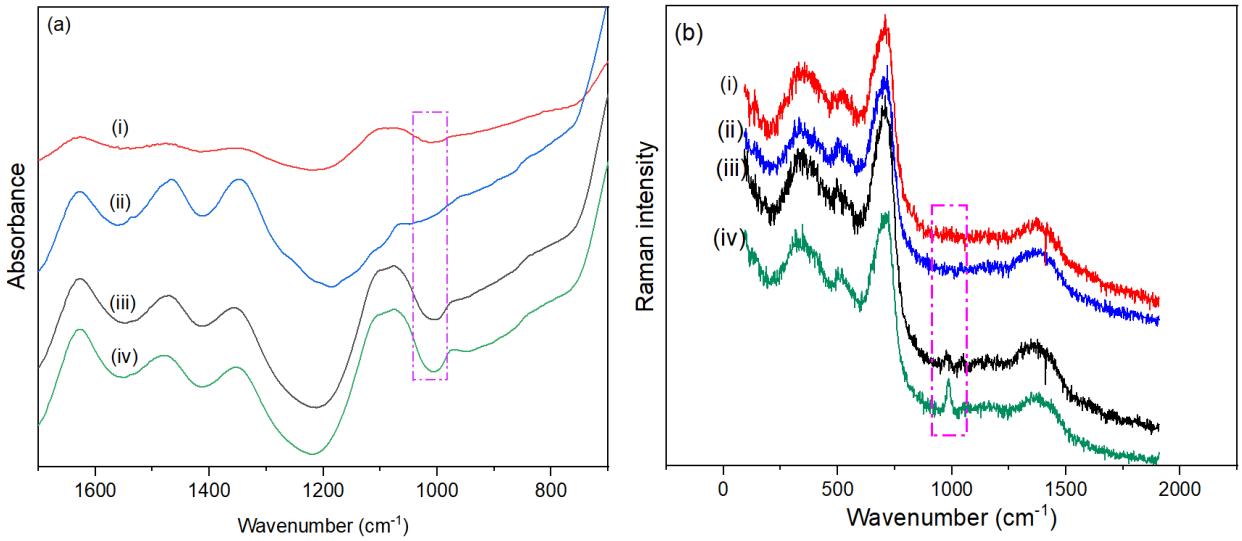

Figure 6: FTIR spectra of CNF-Fe after uptake of (a-i) Cr(VI), (a-ii) As(III), and (a-iii) Cr(VI). Spectra (a-iv) is for the adsorbent prior to exposure to test ions. The boxes highlight changes in the surface -OH absorption region before and after adsorption.

Only a slight change was observed in the Cr(VI) spectra, which corresponds to its much lower adsorption seen in the quantitative results. The sorption of Cr(VI) ions to CNF-Fe is primarily by electrostatic attraction to the Fe-OH_2^+ sites of ferrihydrite (Sannino et al., 2009). Further, chromate complexes are less strongly held (as compared to those of As(V)) and so more easily adsorbed. These factors may have contributed to the lower removal of Cr(VI) ions by CNF-Fe. However, we posit that the presence of sulphate on the adsorbent surface may have had a greater effect as anions have been shown to inhibit the uptake of chromate ions by ferrihydrite (Johnston and Chrysochoou, 2016, 2012; Zhu et al., 2018).

Raman and FTIR data provided insights into changes with respect to sulphate ions in CNF-Fe adsorbent. Sulphate ions (free ions) usually display symmetric stretching at ~983 cm^{-1}, which is both Raman and IR active but more intense in Raman (Rouchon et al., 2012). When bridging adjacent Fe atoms in iron minerals, sulphate ions result in skeletal vibrations of Fe-O-S-O-Fe, producing bands at ~965 cm^{-1} in both IR and Raman spectra. Using both techniques, sulphate ions were shown to be present in the CNF-Fe in both free (Raman: 985 cm^{-1}) and bridging (IR absorption at 970 cm^{-1}) forms.

In the case of Cr(VI) ions, both Raman and IR spectra showed that SO_4^{2-} ions were still present in the adsorbent post-adsorption (Figure 6(b)-iii. However, both Raman and IR data suggest that the concentrations of bridging and free SO_4^{2-} ions at the adsorbent surface were diminished after adsorption of As(III) and As(V) ions Figure 6(a)-i and ii, Figure 6(b)-i and ii. This suggests that SO_4^{2-} ions were exchanged from the adsorbent surface during uptake of As(III) and As(V), but not during Cr(VI) uptake. In fact, SO_4^{2-} ions in the CNF-Fe adsorbent likely inhibited Cr(VI) uptake, through increasing either (i) the electrostatic repulsion at the adsorbent surface (ii) competition for sorption sites (Leckie, J. O. Benjamin, M. M., Hayes, K., Kaufman, G., Altman, 1980; Zachara et al., 1987). Together these data provide insights into the adsorption of As(III), As(V) and Cr(VI) by the synthesised CNF-Fe adsorbent, and possible optimisation strategies for improved removal, particularly of Cr(VI) ions.

Preprints (www.preprints.org) | NOT PEER-REVIEWED | Posted: 9 October 2020 doi:10.20944/preprints202010.0190.v1

iv. Application to mine drainage contaminated water

Batch studies

CNF-Fe adsorbents were applied for the removal of As and Cr from AMD-contaminated water. The results of experiments conducted for 240 minutes without any pH adjustments to the water are presented in Figure 7 below. The data show that up to 39 % of Cr(VI) was removed from solution but that As removal was at 100%. We posit that the low Cr(VI) uptake is due to competitive effects from the high concentrations of sulphate ions typical of AMD, as well as the presence of selenium. Wu et al. found that at high pH selenite ions inhibited Cr(VI) uptake on alumina surfaces. As such, the effective application of these adsorbents would require pre-treatment steps involving removal of sulphate and selenium ions.

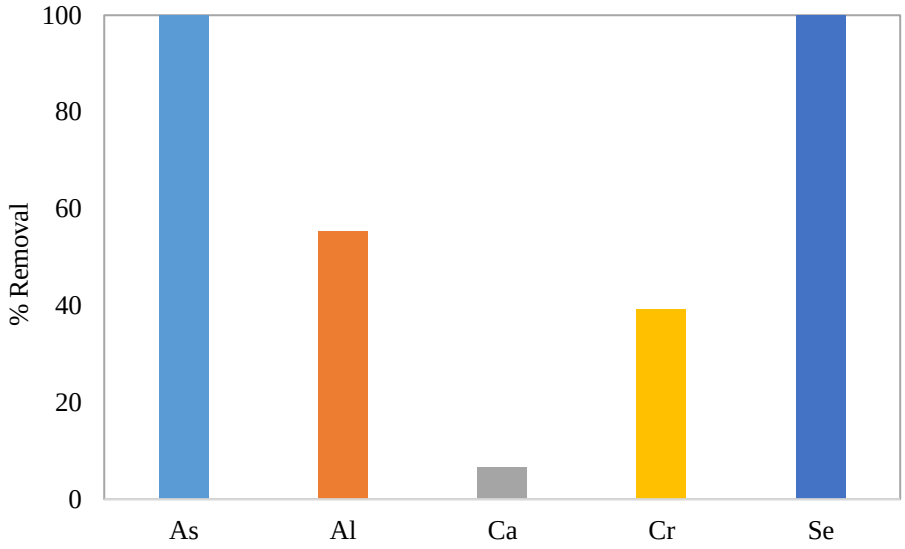

Figure 7: Removal of Arsenic, chromium, and other ions from mine drainage contaminated water by CNF-Fe. Conditions: pH = 2.7, adsorbent mass = 0.03 g, Volume = 25 mL, contact time = 240 minutes.

Column studies

To further examine the applicability of the CNF-Fe adsorbents in water treatment, column studies were conducted. The aim was to examine exhaustion of CNF-Fe adsorbents i.e. the volume of water that could be treated before efficiency of As and Cr removal began to decline. To this end, AMD-contaminated water was filtered through 1 g of adsorbent packed in a glass vial (13 mm diameter). To limit the loss of CNF-Fe into treated water, pure cellulose fibres (1 g) were also packed at the bottom of the vial (Figure 8b).

The results showed that just as with batch studies, uptake of As was higher than Cr (Figure 8a). Removal of Cr did not change much after the first 25 mL, suggesting that after passage of this volume through the filter, competition from selenium and sulphate ions limited Cr uptake to some extent. However, in contrast to As, Cr uptake did not diminish after 250 mL. This would suggest that Cr continued to be taken up by the adsorbent albeit at very low concentrations due to competition. In contrast, As binding sites were saturated from~ 250 mL, allowing escape of the anion through to the filtrate.

These results support those of batch studies by showing that treatments to reduce competitor ions are necessary to improve Cr uptake by CNF-Fe adsorbent. However, they also contribute new insights into adsorbent exhaustion especially with respect to As, that were not apparent from batch studies. They show that adsorbent performance begins

Preprints (www.preprints.org) | NOT PEER-REVIEWED | Posted: 9 October 2020 doi:10.20944/preprints202010.0190.v1

to decay after 250 mL of filtrate when 1g of adsorbent is used and provide a basis for the determination of the appropriate adsorbent mass required for larger volumes of water.

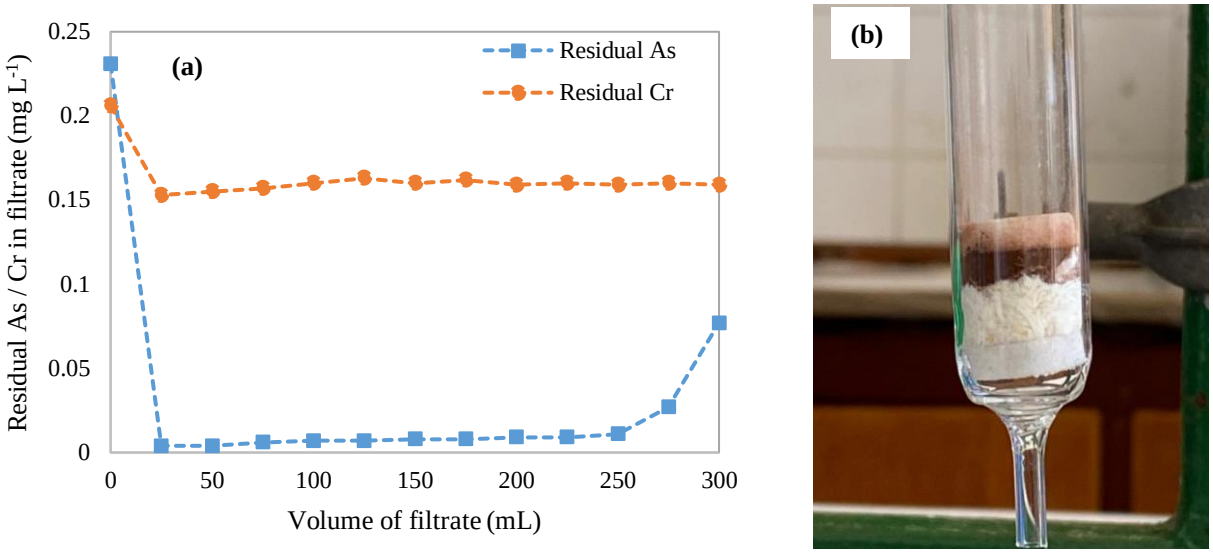

Figure 8: (a) As and Cr in filtrate from column studies. Conditions: *Co* = 0.230 mg L^{-1} for As, 0.206 mg L^{-1} for Cr, adsorbent mass = 1g, solution pH = 2.7, flow rate = 5 min mL^{-1}. **(b)** Photograph of column showing CNF-Fe adsorbent and pure cellulose packed at the base to limit adsorbent loss to treated water.

Desorption studies

Desorption experiments were performed to determine the reversibility of As and Cr adsorption on CNF-Fe sorbent. The results showed that up to 0.209 mg L^{-1} As and 0.04 mg L^{-1} Cr could be desorbed after treatment of the adsorbent with 5.7 mL glacial acid in 1 L of water (Figure 9). This suggests that this extraction fluid is an effective desorption agent for the regeneration of CNF-Fe. However, as the extraction efficiency is far lower for Cr, an additional step, using a more effective desorbent would be required. Nevertheless, these data suggest that the adsorbent can be re-used and that regeneration requires only small amounts of an affordable and readily available desorbent.

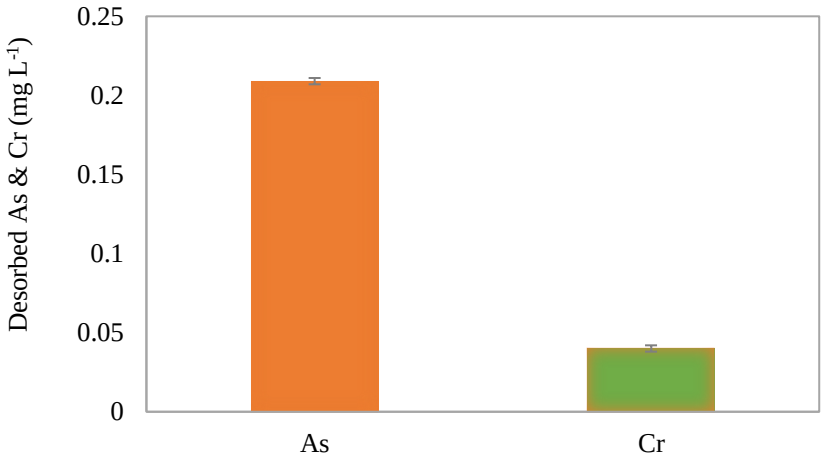

Figure 9: Desorption of As and Cr from CNF-Fe sorbent. Conditions: adsorbent mass = 1.98g, extraction volume = 25 mL, pH = 2.88, time = 24 hours.

Conclusion

This work examined the efficiency of cellulose-supported ferrihydrites (CNF-Fe) in removing of As(III), As(V) and Cr(VI) from synthetic and actual AMD-contaminated water. The results showed that CNF-Fe composites were effective adsorbents for removal of these ions and that while in single-ion solutions adsorption was higher for chromium that arsenic ions, in AMD, competition from sulphate and selenium ions greatly reduced Cr removal efficiency. Desorption experiments showed that the adsorbent can be regenerated be desorption using a cheap and readily available acetic acid, making this an affordable and recyclable water treatment option in low-income settings.

Acknowledgements

We thank Rudolph Erasmus for help with Raman experiments. AE acknowledges funding from the Royal Society under the FLAIR program, contract FLR\R1\190087.

Conflict of interest

The authors declare no conflict of interest

References

Acharya, S., Abidi, N., Rajbhandari, R., Meulewaeter, F., 2014. Chemical cationization of cotton fabric for improved dye uptake. Cellulose 21, 4693–4706. https://doi.org/10.1007/s10570-014-0457-2

Aharoni, C., Ungarish, M., 1977. Kinetics of activated chemisorption. Part 2.-Theoretical models. J. Chem. Soc. Faraday Trans. 1 73, 456–464. https://doi.org/10.1039/F19777300456

Aredes, S., Klein, B., Pawlik, M., 2013. The removal of arsenic from water using natural iron oxide minerals. J. Clean. Prod. 60, 71–76. https://doi.org/10.1016/j.jclepro.2012.10.035

Burton, E.D., Bush, R.T., Johnston, S.G., Watling, K.M., Hocking, R.K., Sullivan, L.A., Parker, G.K., 2009. Sorption of Arsenic(V) and Arsenic(III) to schwertmannite. Environ. Sci. Technol. 43, 9202–9207. https://doi.org/10.1021/es902461x

Chai, F., Wang, R., Yan, L., Li, G., Cai, Y., Xi, C., 2020. Facile fabrication of pH-sensitive nanoparticles based on nanocellulose for fast and efficient As(V) removal. Carbohydr. Polym. 245, 116511. https://doi.org/10.1016/j.carbpol.2020.116511

Coates, J., 2004. Interpretation of Infrared Spectra, A Practical Approach, in: Myers, R.A. (Ed.), Encyclopedia of Analytical Chemistry. John Wiley & Sons Ltd, pp. 1–23.

Davis, J. a., Leckie, J.O., 1978. Effect of adsorbed complexing ligands on trace metal uptake by hydrous oxides. Environ. Sci. Technol. 12, 1309–1315. https://doi.org/10.1021/es60147a006

Eggleton, R.A., Fitzpatrick, R.W., 1988. New Data and a Revised Structural Model for Ferrihydrite. Clays Clay Miner. 36, 111–124. https://doi.org/10.1346/CCMN.1988.0360203

Espinosa, S.C., Kuhnt, T., Foster, E.J., Weder, C., 2013. Isolation of Thermally Stable Cellulose Nanocrystals by Phosphoric Acid Hydrolysis. Biomacromolecules 14, 1223–1230. https://doi.org/10.1021/bm400219u

Foster, E.J., Moon, R.J., Agarwal, U.P., Bortner, M.J., Bras, J., Camarero-espinosa, S., Fox, D.M., Hamad, W.Y., Heux, L., Jean, B., Korey, M., Nieh, W., Ong, K.J., Reid, M.S., Renneckar, S., Roberts, R., Shatkin, J.A.,

Simonsen, J., Stinson-Bagby, K., Wanasekera, N., Youngblood, J., 2018. Current characterization methods for cellulose nanomaterials. Chem. Soc. Rev. 47, 2609–2679. https://doi.org/10.1039/c6cs00895j

Goetz, L.A., Naseri, N., Nair, S.S., Karim, Z., Mathew, A.P., 2018. All cellulose electrospun water purification membranes nanotextured using cellulose nanocrystals. Cellulose 25, 3011–3023. https://doi.org/10.1007/s10570-018-1751-1

Gray, J.E., Theodorakos, P.M., Bailey, E. a, Turner, R.R., 2000. Distribution, speciation, and transport of mercury in stream-sediment, stream-water, and fish collected near abandoned mercury mines in southwestern Alaska, USA. Sci. Total Environ. 260, 21–33.

Hansen, H.K., Núñez, P., Grandon, R., 2006. Electrocoagulation as a remediation tool for wastewaters containing arsenic. Miner. Eng. 19, 521–524. https://doi.org/10.1016/j.mineng.2005.09.048

Hirota, M., Tamura, N., Saito, T., Isogai, A., 2010. Water dispersion of cellulose II nanocrystals prepared by TEMPO-mediated oxidation of mercerized cellulose at pH 4.8. Cellulose 17, 279–288. https://doi.org/10.1007/s10570-009-9381-2

Ho, Y.S., Mckay, G., 2004. Sorption of copper(II) from aqueous solution by peat. Water Air Soil Pollut. 158, 77–97. https://doi.org/10.1023/B:WATE.0000044830.63767.a3

Hutson, N.D., Yang, R.T., 1997. Theoretical Basis for the Dubinin-Radushkevitch (D-R) Adsorption Isotherm Equation 195, 189–195.

Isogai, A., Saito, T., Fukuzumi, H., 2011. TEMPO-oxidised cellulose nanofibers. Nanoscale 3, 71–85. https://doi.org/10.1039/c0nr00583e

Jain, A., Raven, K.P., Loeppert, R.H., 1999. Arsenite and arsenate adsorption on ferrihydrite: Surface charge reduction and net OH- release stoichiometry. Environ. Sci. Technol. 33, 1179–1184. https://doi.org/10.1021/es980722e

Ji, H., Xiang, Z., Qi, H., Han, T., Pranovich, A., Song, T., 2019. Strategy towards one-step preparation of carboxylic cellulose nanocrystals and nanofibrils with high yield, carboxylation and highly stable dispersibility using innocuous citric acid. Green Chem. 21, 1956–1964. https://doi.org/10.1039/c8gc03493a

Johnston, C.P., Chrysochoou, M., 2016. Mechanisms of Chromate, Selenate, and Sulfate Adsorption on Al-Substituted Ferrihydrite: Implications for Ferrihydrite Surface Structure and Reactivity. Environ. Sci. Technol. 50, 3589–3596. https://doi.org/10.1021/acs.est.5b05529

Johnston, C.P., Chrysochoou, M., 2012. Investigation of chromate coordination on ferrihydrite by in situ ATR-FTIR spectroscopy and theoretical frequency calculations. Environ. Sci. Technol. 46, 5851–5858. https://doi.org/10.1021/es300660r

Kleinert, S., Muehe, E.M., Posth, N.R., Dippon, U., Daus, B., Kappler, A., 2011. Biogenic Fe(III) minerals lower the efficiency of iron-mineral-based commercial filter systems for arsenic removal. Environ. Sci. Technol. 45, 7533–7541. https://doi.org/10.1021/es201522n

Klemm, D., Heublein, B., Fink, H.P., Bohn, A., 2005. Cellulose: Fascinating biopolymer and sustainable raw material. Angew. Chemie - Int. Ed. 44, 3358–3393. https://doi.org/10.1002/anie.200460587

Leckie, J. O. Benjamin, M. M., Hayes, K., Kaufman, G., Altman, S., 1980. Adsorption/Coprecipitation of Trace Elements from Water with Iron Oxyhydroxide 1–270.

Mamindy-Pajany, Y., Hurel, C., Marmier, N., Roméo, M., 2011. Arsenic (V) adsorption from aqueous solution onto goethite, hematite, magnetite and zero-valent iron: Effects of pH, concentration and reversibility. Desalination 281, 93–99. https://doi.org/10.1016/j.desal.2011.07.046

Mautner, A., Kwaw, Y., Weiland, K., Mvubu, M., Botha, A., John, M.J., Mtibe, A., Siqueira, G., Bismarck, A., 2019. Natural fibre-nanocellulose composite filters for the removal of heavy metal ions from water. Ind. Crops Prod. 133, 325–332. https://doi.org/10.1016/j.indcrop.2019.03.032

Mazzetti, L., Thistlethwaite, P.J., 2002. Raman spectra and thermal transformations of ferrihydrite and schwertmannite. J. Raman Spectrosc. 33, 104–111. https://doi.org/10.1002/jrs.830

Michel, F.M., Barrón, V., Torrent, J., Morales, M.P., Serna, C.J., Boily, J.F., Liu, Q., Ambrosini, A., Cismasu, A.C., Brown, G.E., 2010. Ordered ferrimagnetic form of ferrihydrite reveals links among structure, composition, and magnetism. Proc. Natl. Acad. Sci. U. S. A. 107, 2787–2792. https://doi.org/10.1073/pnas.0910170107

Montanari, S., Roumani, M., Heux, L., Vignon, M.R., 2005. Topochemistry of carboxylated cellulose nanocrystals resulting from TEMPO-mediated oxidation. Macromolecules 38, 1665–1671. https://doi.org/10.1021/ma048396c

Morrison, S.J., Metzler, D.R., Dwyer, B.P., 2002. Removal of As, Mn, Mo, Se, U, V and Zn from groundwater by zero-valent iron in a passive treatment cell: reaction progress modeling. J. Contam. Hydrol. 56, 99–116. https://doi.org/10.1016/S0169-7722(01)00205-4

Mukherjee, S., Kumar, A.A., Sudhakar, C., Kumar, R., Ahuja, T., Mondal, B., Srikrishnarka, P., Philip, L., Pradeep, T., 2019. Sustainable and Affordable Composites Built Using Microstructures Performing Better than Nanostructures for Arsenic Removal. ACS Sustain. Chem. Eng. 7, 3222–3233. https://doi.org/10.1021/acssuschemeng.8b05157

Müller, K., Ciminelli, V.S.T., Dantas, M.S.S., Willscher, S., 2010. A comparative study of As(III) and As(V) in aqueous solutions and adsorbed on iron oxy-hydroxides by Raman spectroscopy. Water Res. 44, 5660–5672. https://doi.org/10.1016/j.watres.2010.05.053

Naicker, K., Cukrowska, E., McCarthy, T.S., 2003. Acid mine drainage arising from gold mining activity in Johannesburg, South Africa and environs. Environ. Pollut. 122, 29–40. https://doi.org/10.1016/S0269-7491(02)00281-6

Newcombe, R.L., Strawn, D.G., Grant, T.M., Childers, S.E., Möller, G., 2008. Phosphorus Removal from Municipal Wastewater by Hydrous Ferric Oxide Reactive Filtration and Coupled Chemically Enhanced Secondary Treatment: Part II-Mechanism. Water Environ. Res. 80, 248–256. https://doi.org/10.2175/106143007x220987

Nordstrom, D.K., 2002. Worldwide occurrences of arsenic in ground water. Science (80-.). 296, 2143–2145. https://doi.org/10.1126/science.1072375

Nordstrom, D.K., Alpers, C.N., Ptacek, C.J., Blowes, D.W., 2000. Negative pH and extremely acidic mine waters from Iron Mountain, California. Environ. Sci. Technol. 34, 254–258. https://doi.org/10.1021/es990646v

Raven, K.P., Jain, A., Loeppert, R.H., 1998. Arsenite and arsenate adsorption on ferrihydrite: Kinetics, equilibrium, and adsorption envelopes. Environ. Sci. Technol. 32, 344–349. https://doi.org/10.1021/es970421p

Rouchon, V., Badet, H., Belhadj, O., Bonnerot, O., Lavódrine, B., Michard, J.G., Miska, S., 2012. Raman and FTIR spectroscopy applied to the conservation report of paleontological collections: Identification of Raman and FTIR signatures of several iron sulfate species such as ferrinatrite and sideronatrite. J. Raman Spectrosc. 43, 1265–1274. https://doi.org/10.1002/jrs.4041

Rout, K., Mohapatra, M., Anand, S., 2012. 2-Line ferrihydrite: Synthesis, characterization and its adsorption behaviour for removal of Pb(II), Cd(II), Cu(II) and Zn(II) from aqueous solutions. Dalt. Trans. 41, 3302–3312. https://doi.org/10.1039/c2dt11651k

Russel, J.D., 1979. Infrared spectroscopy of ferrihydrite: evidence for the presence of structural hydroxyl groups. Clay Miner. 14, 109–114.

Saha, R., Nandi, R., Saha, B., 2011. Sources and toxicity of hexavalent chromium. J. Coord. Chem. 64, 1782–1806. https://doi.org/10.1080/00958972.2011.583646

Saito, T., Kimura, S., Nishiyama, Y., Isogai, A., 2007. Cellulose Nanofibers Prepared by TEMPO-Mediated Oxidation of Native Cellulose. Biomacromolecules 8, 2485–2491. https://doi.org/10.1021/BM0703970

Sannino, F., Martino, A. De, Pigna, M., Violate, A., Leo, P. Di, Mesto, E., Capasso, R., 2009. Sorption of arsenate and dichromate on polymerin, Fe(OH)x-polymerin complex and ferrihydrite. J. Hazard. Mater. 166, 1174–

1179.

Schwertmann, U., Fechter, H., 1982. The point of zero charge of natural and synthetic ferrihydrites and its relation to adsorbed silicate. Clay Miner. 17, 471–476. https://doi.org/10.1180/claymin.1982.017.4.10

Sehaqui, H., Kulasinski, K., Pfenninger, N., Zimmermann, T., Tingaut, P., 2016. Highly Carboxylated Cellulose Nanofibers via Succinic Anhydride Esterification of Wheat Fibers and Facile Mechanical Disintegration. https://doi.org/10.1021/ACS.BIOMAC.6B01548

Sehaqui, Houssine, Mautner, A., Perez De Larraya, U., Pfenninger, N., Tingaut, P., Zimmermann, T., 2016. Cationic cellulose nanofibers from waste pulp residues and their nitrate, fluoride, sulphate and phosphate adsorption properties. Carbohydr. Polym. 135, 334–340. https://doi.org/10.1016/j.carbpol.2015.08.091

Shateri Khalil-Abad, M., Yazdanshenas, M.E., Nateghi, M.R., 2009. Effect of cationization on adsorption of silver nanoparticles on cotton surfaces and its antibacterial activity. Cellulose 16, 1147–1157. https://doi.org/10.1007/s10570-009-9351-8

Shinoda, R., Saito, T., Okita, Y., Isogai, A., 2012. Relationship between length and degree of polymerization of TEMPO-oxidized cellulose nanofibrils. Biomacromolecules 13, 842–849. https://doi.org/10.1021/bm2017542

Silvério, H.A., Flauzino Neto, W.P., Dantas, N.O., Pasquini, D., 2013. Extraction and characterization of cellulose nanocrystals from corncob for application as reinforcing agent in nanocomposites. Ind. Crops Prod. 44, 427–436. https://doi.org/10.1016/j.indcrop.2012.10.014

Smedley, P.L., Kinniburgh, D.G., 2002. A review of the source, behaviour and distribution of arsenic in natural waters. Appl. Geochemistry 17, 517–568. https://doi.org/10.1016/S0883-2927(02)00018-5

Smith, E., Ghiassi, K., 2006. Chromate Removal by an Iron Sorbent: Mechanism and Modeling. Water Environ. Res. 78, 84–93. https://doi.org/10.2175/106143005x84558

Thommes, M., Kaneko, K., Neimark, A. V., Olivier, J.P., Rodriguez-Reinoso, F., Rouquerol, J., Sing, K.S.W., 2015. Physisorption of gases, with special reference to the evaluation of surface area and pore size distribution (IUPAC Technical Report). Pure Appl. Chem. 87, 1051–1069. https://doi.org/10.1515/pac-2014-1117

Tutu, H., 2006. Determination and geochemical modelling of the dispersal of uranium in gold-mine polluted land on the Witwatersrand Basin. University of the Witwatersrand.

Tutu, R.A., Stoler, J., 2016. Urban but off the grid: the struggle for water in two urban slums in greater Accra, Ghana. African Geogr. Rev. 35, 212–226. https://doi.org/10.1080/19376812.2016.1168309

Udoetok, I.A., Dimmick, R.M., Wilson, L.D., Headley, J. V., 2016. Adsorption properties of cross-linked cellulose-epichlorohydrin polymers in aqueous solution. Carbohydr. Polym. 136, 329–340. https://doi.org/10.1016/j.carbpol.2015.09.032

USEPA, 1992. Test method for evaluation of solid waste, physical/chemical methods SW 846 [WWW Document]. Method 1311, Toxic. Charact. leaching Proced.

Wang, X., Li, W., Harrington, R., Liu, F., Parise, J.B., Feng, X., Sparks, D.L., 2013. Effect of ferrihydrite crystallite size on phosphate adsorption reactivity. Environ. Sci. Technol. 47, 10322–10331. https://doi.org/10.1021/es401301z

Waychunas, G.A., Rea, B.A., Fuller, C.C., Davis, J.A., 1993. Surface chemistry of ferrihydrite: Part 1. EXAFS studies of the geometry of coprecipitated and adsorbed arsenate. Geochim. Cosmochim. Acta 57, 2251–2269. https://doi.org/10.1016/0016-7037(93)90567-G

WHO, 2019. Preventing Disease through Healthy Environment. Exposure to Arsenic: A Major Public Health Concern. Prev. Dis. through Heal. Environ. 1–5.

World Health Organization, 2011. WHO guidelines for drinking-water quality, 4th Edition, WHO chronicle. Geneva.

Zachara, J.M., Girvin, D.C., Schmidt, R.L., Resch, C.T., 1987. Chromate Adsorption on Amorphous Iron Oxyhydroxide in the Presence of Major Groundwater Ions. Environ. Sci. Technol. 21, 589–594. https://doi.org/10.1021/es00160a010

Zaman, M., Xiao, H., Chibante, F., Ni, Y., 2012. Synthesis and characterization of cationically modified nanocrystalline cellulose. Carbohydr. Polym. 89, 163–170. https://doi.org/10.1016/j.carbpol.2012.02.066

Zhou, Y., Saito, T., Isogai, A., 2018. Acid-Free Preparation of Cellulose Nanocrystals by TEMPO Oxidation and Subsequent Cavitation. https://doi.org/10.1021/acs.biomac.7b01730

Zhu, C., Soldatov, A., Mathew, A.P., 2017. Advanced microscopy and spectroscopy reveal the adsorption and clustering of Cu(II) onto TEMPO-oxidized cellulose nanofibers. Nanoscale 9, 7419–7428. https://doi.org/10.1039/c7nr01566f

Zhu, L., Fu, F., Tang, B., 2018. Coexistence or aggression? Insight into the influence of phosphate on Cr(VI) adsorption onto aluminium-substituted ferrihydrite. Chemosphere 212, 408–417.